JOURNAL OF VIROLOGY, Oct. 2010, p. 10276–10288 Vol. 84, No. 19
0022-538X/10/$12.00 doi:10.1128/JVI.01287-10

An Interaction between the Nucleocapsid Protein and a Component of the Replicase-Transcriptase Complex Is Crucial for the Infectivity of Coronavirus Genomic RNA▽

Kelley R. Hurst,[1] Rong Ye,[1]† Scott J. Goebel,[1] Priya Jayaraman,[2] and Paul S. Masters[1,2]*

Wadsworth Center, New York State Department of Health,[1] and Department of Biomedical Sciences, The University at Albany, State University of New York,[2] Albany, New York 12201

Received 16 June 2010/Accepted 14 July 2010

The coronavirus nucleocapsid (N) protein plays an essential role in virion assembly via interactions with the large, positive-strand RNA viral genome and the carboxy-terminal endodomain of the membrane protein (M). To learn about the functions of N protein domains in the coronavirus mouse hepatitis virus (MHV), we replaced the MHV N gene with its counterpart from the closely related bovine coronavirus (BCoV). The resulting viral mutant was severely defective, even though individual domains of the N protein responsible for N-RNA, N-M, or N-N interactions were completely interchangeable between BCoV and MHV. The lesion in the BCoV N substitution mutant could be compensated for by reverting mutations in the central, serine- and arginine-rich (SR) domain of the N protein. Surprisingly, a second class of reverting mutations were mapped to the amino terminus of a replicase subunit, nonstructural protein 3 (nsp3). A similarly defective MHV N mutant bearing an insertion of the SR region from the severe acute respiratory syndrome coronavirus N protein was rescued by the same two classes of reverting mutations. Our genetic results were corroborated by the demonstration that the expressed amino-terminal segment of nsp3 bound selectively to N protein from infected cells, and this interaction was RNA independent. Moreover, we found a direct correlation between the N-nsp3 interaction and the ability of N protein to stimulate the infectivity of transfected MHV genomic RNA (gRNA). Our results suggest a role for this previously unknown N-nsp3 interaction in the localization of genomic RNA to the replicase complex at an early stage of infection.

For positive-strand RNA viruses, genomic RNA (gRNA) functions both as a message for translation and as a template for the viral RNA-dependent RNA polymerase. As part of their infectious cycle, these viruses often extensively remodel host cellular membranous compartments to facilitate replication and transcription of gRNA. These expropriated membranes are thought to provide surfaces for the concentration of enzymatic and substrate components of RNA synthesis, to furnish general protection from cellular ribonucleases, and to allow evasion of host innate immunity through the sequestration of double-stranded viral RNA intermediates. Among all known RNA viruses, coronaviruses have the largest genomes, ranging from 27 to 32 kb, and the most complex machinery for RNA synthesis (21, 35, 74). The coronavirus replicase-transcriptase complex (here called the replicase) is assembled from 16 nonstructural proteins (nsp), which collectively total some 803 kDa for mouse hepatitis virus (MHV). The nsp are autoproteolytically processed from two overlapping polyprotein precursors, which are produced by translation of gRNA. Almost all of the replicase components are associated with or embedded in convoluted membranes and double-membrane vesicles that are generated during coronavirus infection (29).

In addition to the replicase, the nucleocapsid protein (N) is known to play an important role in coronavirus RNA synthesis, although that role is, as yet, poorly defined (1, 51, 60, 76). Multiple investigations have shown intracellular colocalization of N with replicase components at early stages of infection by MHV or by severe acute respiratory syndrome coronavirus (SARS-CoV) (14, 55, 58, 61). The participation of N protein in an early event in RNA synthesis is also implied by the poor adherence of coronaviruses to the nearly universal rule that the gRNA of positive-strand RNA viruses is completely infectious when introduced into susceptible host cells. Some time ago, we noted that the infectivity of purified MHV gRNA was markedly enhanced by cotransfection of synthetic N mRNA (36); this phenomenon was rediscovered when full-length reverse-genetic systems were devised for coronaviruses. For systems that are launched by transfection of gRNA, the provision of cotransfected N mRNA or N-encoding plasmid either is greatly stimulatory (10, 69–71) or is absolutely required (6) for the recovery of infectious virus.

In the present study, we analyzed the consequences of replacing the MHV N open reading frame (ORF) with its counterpart from the closely related bovine coronavirus (BCoV). This substitution resulted in the discovery of a previously unsuspected genetic interaction between the serine- and arginine-rich (SR) region of the N protein and a region of the nsp3 subunit of the viral replicase. We confirmed this interaction through biochemical pulldown experiments. Moreover, we found that there is a correlation between the N-nsp3 interaction and the ability of N protein to stimulate the infectivity of MHV gRNA. Our results offer an explanation for the requirement for N protein in the early events of coronavirus infection.

* Corresponding author. Mailing address: David Axelrod Institute, Wadsworth Center, NYSDOH, New Scotland Avenue, P.O. Box 22002, Albany, NY 12201-2002. Phone: (518) 474-1283. Fax: (518) 473-1326. E-mail: masters@wadsworth.org.

† Present address: Fudan University Shanghai Medical School, 138 Yixueyuan Rd., P.O. Box 168, Shanghai 200032, China.

▽ Published ahead of print on 21 July 2010.

MATERIALS AND METHODS

Viruses and cell lines. Wild-type MHV-A59 and constructed mutants were propagated in mouse 17 clone 1 (17Cl1) cells; plaque assays and plaque purifications of mutants and revertants were carried out using mouse L2 cells. The interspecies chimeric virus designated fMHV.v2 (20, 31) was grown in feline FCWF cells.

Construction of MHV mutants. MHV reverse genetics was carried out through targeted RNA recombination, using the host range-based selection system described in detail previously (20, 31, 37). In brief, monolayers of FCWF cells were infected with fMHV.v2 and then transfected with *in vitro*-synthesized donor RNAs (mMessage mMachine T7; Ambion). Harvested progeny virus was selected and purified by plaque titration on mouse L2 cells. The presence of incorporated genes, gene fragments, or mutations in candidate recombinants was confirmed by sequencing of reverse transcription (RT)-PCR products obtained from viral RNA.

Transcription vectors for the synthesis of donor RNAs were derived from pMH54 (31) or pSG6 (20), each of which contains 5′ elements of the MHV-A59 genome linked to the 3′-most 8.6 kb of the MHV-A59 genome; pSG6 is identical to pMH54, except for a coding-silent BspEI site spanning codons 444 to 446 of the N gene. Substitutions of N gene regions from other coronaviruses were made from a BCoV N gene plasmid, pLN, which was originally obtained from David Brian (University of Tennessee) (43, 52), or from SARS-CoV plasmid pMSARS-1, which is a cDNA clone of the N gene of SARS-CoV strain Urbani. Fragments of the human coronavirus HKU1 (HCoV-HKU1) N gene were synthesized from overlapping oligonucleotides by PCR.

For domain N3 constructs, a subclone of pSG6, pN-sub, which removed all MHV sequence upstream of the Bsu36I site in the N gene, was generated. Plasmids containing BCoV, HCoV-HKU1, or SARS-CoV domain N3 substitutions were constructed in pN-sub via replacement of the MHV N gene BsmI-BstEII fragment, running from the start of spacer B through the upstream end of the 3′ untranslated region (UTR). Downstream PCR primers for these substitutions were designed such that the MHV 3′ UTR was left unaltered. The NheI-PacI fragment of each subclone was then used to replace the corresponding fragment of pMH54 to generate transcription vectors pMH54-BN3, pMH54-HKN3, and pMH54-SN3.

Transcription vector pMH54-BCVN, containing an exact replacement of the MHV N ORF by the BCoV N ORF, was constructed from segments of pMH54-BN3 and the previously described plasmid pTM1 (43), following an intermediate step that generated an MHV M-BCoV N intergenic junction in pTM1. An MHV-BCoV N gene duplication vector, pMH54-MB, was created from pMH54-BCVN by transfer from pA122 of the SbfI-BssHII fragment, running from downstream of the S gene through the M gene. The previously described plasmid pA122 (13) contains a single copy of the N gene transposed to the position occupied by gene 4 in the wild-type MHV genome. It should be noted that the upstream copy of the MHV N gene in pMH54-MB is not epitope-tagged, unlike its MHV-MHV N duplication counterpart, pA112 (27).

Transcription vector pMH54-HKSR5, containing the SR region of the HCoV-HKU1 N gene, was made through a subclone intermediate, pPJ1, which contained the M and N genes of pSG6. Following replacement of the ApaI-NgoMIV fragment of pPJ1, the BssHII-BspEI fragment of the resulting plasmid was transferred back to pSG6. Transcription vector pMH54-SSR6, containing the SR region of the SARS-CoV N gene, was constructed by a similar strategy, through replacement of the Bsu36I-NgoMIV fragment of pPJ1.

All DNA cloning and manipulations were carried out by standard techniques. Oligonucleotides for PCR, gene fragment construction, and DNA sequencing were obtained from Integrated DNA Technologies. The compositions of all plasmid constructs were initially verified by restriction analysis. Final confirmation was established by DNA sequencing of PCR-generated segments, cloned cDNA precursors, and reconstructed or newly created junctions of each plasmid.

Revertant analysis. Independent revertants (designated rev1 through rev14) of the BCoV N mutant were isolated in three separate searches. Rev6 was identified as a large plaque obtained from a fast-growing passage 1 stock (at 37°C) begun from a small plaque from the targeted-RNA-recombination experiment that produced the original BCoV N mutant, Alb613. Each of the other revertants was individually obtained from a stock that was begun from an independent tiny plaque of Alb613; the stock was propagated for three to six passages at 37°C or 39°C, and a single revertant was isolated as a large plaque. For rev1 through rev13, RT-PCR products obtained from purified infected cell RNA were used to determine the sequence of the entire BCoV N ORF (and flanking regions of the upstream M ORF and downstream 3′ UTR) as well as of the region encoding the carboxy-terminal 88 amino acids of nsp2 through the 612 amino-terminal amino acids of nsp3. For rev14, overlapping RT-PCR amplicons spanning the entire genome were sequenced at least once on each strand. The extreme 3′ end of the genome was confirmed through TA cloning and sequencing of RT-PCR products running from the 3′ UTR through the poly(A) tail. The extreme 5′-end genomic sequence was obtained by rapid amplification of cDNA ends (RACE) (5′ RACE system; Invitrogen), followed by TA cloning and sequencing. For reconstruction of the S202L and S205P revertants, the XbaI-NsiI fragment of either pB60SL or pB60SP (see below) was used to replace the corresponding fragment of transcription vector pMH54-BCVN.

Pulldown assay. The region encoding the amino-terminal segment of nsp3 (amino acids 1 to 273) was cloned as a glutathione *S*-transferase (GST) fusion protein gene in pGEX6P (Pharmacia). GST-nsp3(1-273) and GST were expressed in *Escherichia coli* Rosetta pLysS cells (Novagen), following induction with 1 mM IPTG (isopropyl-β-D-thiogalactopyranoside) at 20°C for 18 h. Bacteria were harvested, resuspended in TBS buffer (25 mM Tris-HCl, pH 7.4, 150 mM NaCl) containing 5 mM dithiothreitol (DTT) and protease inhibitors (0.7 μg/ml pepstatin, 1.0 μg/ml leupeptin, 1.0 μg/ml aprotinin, and 0.5 mg/ml Pefabloc SC [Roche]), and lysed by sonication on ice. Bacterial lysates were clarified by centrifugation.

For preparation of control or infected cell lysates, nearly confluent monolayers of 17Cl1 cells were mock infected or infected with wild-type MHV (Alb240) at a multiplicity of 2 PFU per cell. At 8 h postinfection, monolayers were washed twice with TBS and then lysed by addition of 50 mM Tris-HCl, pH 8.0, 150 mM NaCl, 1.0% NP-40, and protease inhibitors. Lysates were held for 35 min on ice and were then clarified by centrifugation. Supernatants were aliquoted and stored at −80°C until used. RNase A treatment was carried out by incubation of 400 μl of lysate with 2.5 U RNase A (Boehringer Mannheim) for 30 min at 37°C immediately prior to the pulldown assay; precipitate that formed during treatment was removed by brief centrifugation at 4°C.

Pulldown assays were performed using components of the ProFound GST interaction kit (Pierce). Glutathione affinity resin was incubated with GST-nsp3(1-273) or GST bacterial lysates (or a buffer control) for 18 h at 4°C, with gentle end-over-end rotation. Bound resin was washed five times with TBS containing 5 mM DTT at 4°C, and 100-μl aliquots of a 50% slurry of bound resin were distributed to spin columns. Samples (400 μl) of untreated or RNase A-treated control or infected cell lysates were added to columns and incubated for 3 h at 4°C, with gentle end-over-end rotation. Columns were washed five times with TBS containing 5 mM DTT at 4°C. We found the inclusion of DTT in wash buffer to be critical for reducing nonspecific binding of N protein to glutathione affinity resin. Bound protein was eluted with 200 μl of 10 mM glutathione in TBS. Aliquots of eluted proteins were then analyzed by SDS-PAGE through 12% polyacrylamide gels, with prestained protein standards (Invitrogen) in flanking lanes, followed by Coomassie blue staining (GelCode Blue; Pierce) or Western blotting. For Western blot analysis, proteins were transferred to polyvinylidene difluoride membranes, and blots were then probed with anti-N protein mouse monoclonal J.3.3 antibody (provided by John Fleming, University of Wisconsin, Madison, WI), anti-N polyclonal rabbit antiserum (26), or anti-GST polyclonal goat antiserum (Amersham). Bound primary antibodies were visualized with a chemiluminescence detection system (ECL; Pierce).

Cotransfection assay. Wild-type MHV gRNA was isolated, via phenol-chloroform extraction and ethanol precipitation, from virions that had been purified by two cycles of equilibrium centrifugation on preformed glycerol-tartrate gradients, as described in detail previously (68). N mRNAs were transcribed from pCK70 or derivatives thereof; pCK70 is a template for an exact copy of wild-type MHV subgenomic RNA7 (30, 36). The N ORF of pCK70 was knocked out by PCR mutagenesis, producing vector pCK70KO, which contained the stop codons TAA and TGA replacing codons 9 and 12, respectively; a coding-silent XbaI site was also generated at codons 15 and 16 of the N ORF in pCK70KO. Vector pB60 was derived from pB11 (43) by replacement of its MfeI-HindIII fragment, running from the end of the 3′ UTR through the poly(A) tract, with the corresponding fragment from pCK70. As a result, pB60 is a template for an exact copy of wild-type BCoV N mRNA, except that it contains the 5′ leader segment from MHV N mRNA. Vectors pB60SL and pB60SP, derivatives of pB60 containing the point mutations S202L and S205P, respectively, were constructed through replacement of the Bsu36I-SpeI fragment of pB60 (encompassing the middle third of the N ORF) with Bsu36I-SpeI fragments obtained from RT-PCR products from viral RNAs of the corresponding revertants of the BCoV N mutant.

MHV gRNA and capped synthetic N mRNAs were cotransfected into L2 cells that had been suspended by mild trypsinization, using 2 mg/ml DEAE-dextran (Pharmacia) in IRA buffer (38). After 2 h of incubation at 37°C, cells were seeded into 20-cm^2 dishes. Following 8 h of attachment, medium was removed, agar overlays were applied, and incubation was continued at 37°C. Plaques were counted at 72 h posttransfection. To verify the integrity of synthetic transcripts,

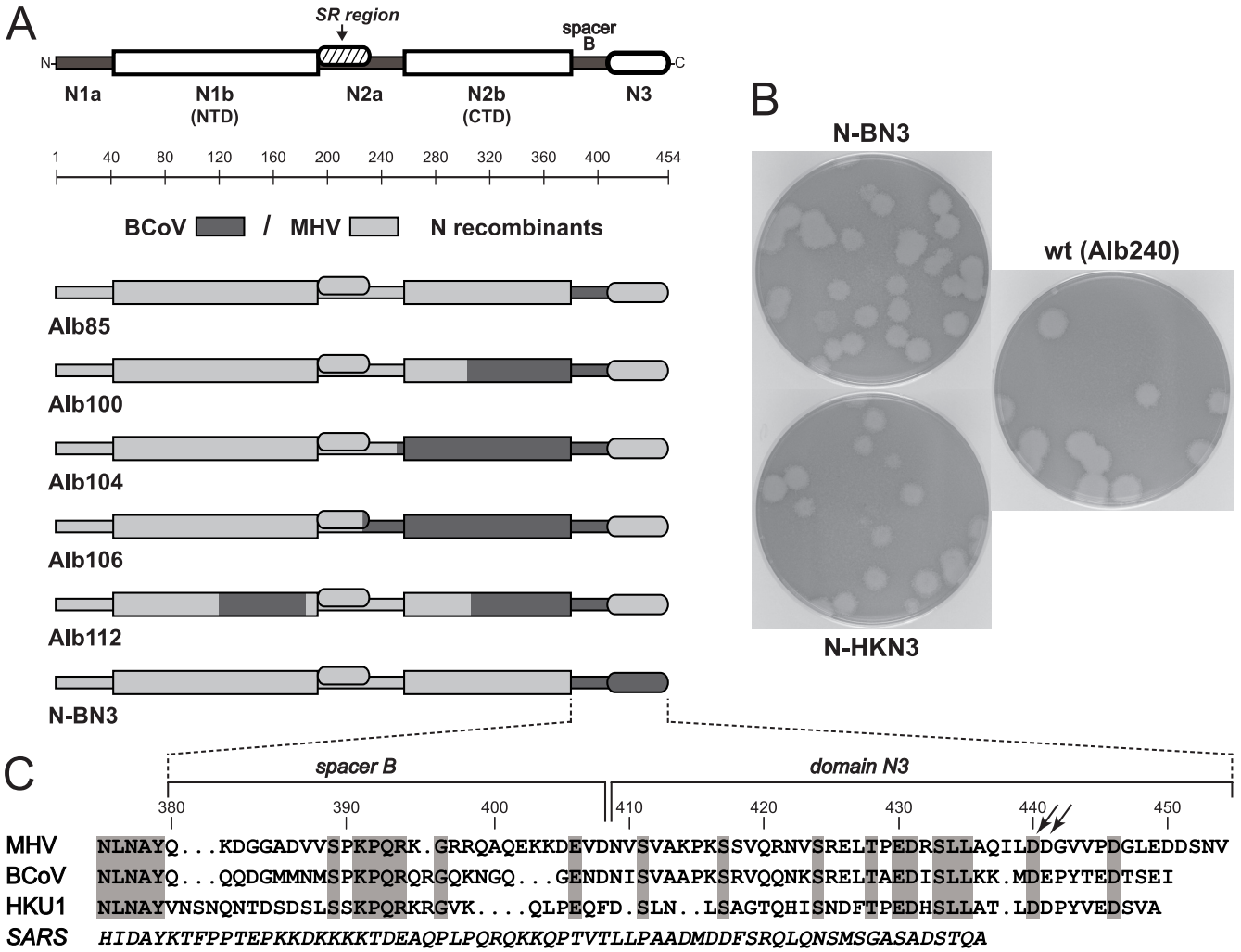

FIG. 1. Tolerated substitutions between the BCoV and MHV N proteins. (A) Schematic of the MHV N protein divided into domains, as demarcated previously (26); our domains N1b and N2b correspond to the RNA-binding NTD and CTD, respectively, defined by others (7, 23). The SR region is denoted within domain N2a. The number line indicates amino acid residues. Beneath is a summary of viable recombinants containing portions of the BCoV N protein (dark shaded areas) substituted for the corresponding regions of the MHV N protein. Recombinants Alb85 to Alb112 were reported previously (43); recombinant N-BN3 is from the current work. (B) Plaques of mutants containing substitutions of N protein spacer B and domain N3 from BCoV (mutant N-BN3) or from HCoV-HKU1 (mutant N-HKN3), compared with wild-type (wt) plaques. The wild-type MHV used throughout this study was Alb240, a well-characterized isogenic recombinant that was previously reconstructed from fMHV and wild-type donor RNA (33). Plaque titrations were carried out on L2 cells at 37°C. Monolayers were stained with neutral red at 96 h postinfection and photographed 18 h later. (C) Amino acid sequence alignment of the carboxy termini of the N proteins of MHV, BCoV, and HCoV-HKU1; the corresponding (unaligned) region of the divergent SARS-CoV N protein is shown for comparison. The residue numbers are for the MHV N sequence; shading denotes residues that are common to the first three proteins. Arrows mark two aspartate residues that are critical for the interaction between the MHV N and M proteins (27, 62). The GenBank accession numbers for the sequences shown are as follows: for MHV-A59, AY700211; for BCoV strain Mebus, U00735; for HCoV-HKU1 genotype A, AY597011; and for SARS-CoV strain Urbani, AY278741.

we translated N mRNAs in a rabbit reticulocyte lysate (Ambion) labeled with [^{35}S]methionine (MP Biomedicals), and protein products were analyzed by SDS-PAGE, followed by fluorography.

RESULTS

Functional equivalence of N3 domains among N proteins of group 2a coronaviruses. The MHV N protein comprises multiple domains (Fig. 1A) that have been defined through our previous genetic studies (27, 30, 32) and through extensive structural studies by others (see reference 26 and references therein). The structured domains, N1b (corresponding to the N-terminal domain [NTD]) and N2b (corresponding to the C-terminal domain [CTD]), fold independently and possess RNA-binding activity. These are bounded by the amino-terminal domain N1a, the centrally located domain N2a, and the carboxy-terminal spacer B and domain N3. Within domain N2a is the SR region, a serine- and arginine-rich tract, which we previously noted to resemble the SR domains of splicing factors (43). In an early study of the N protein, we sought to determine which segments of the MHV N protein could be functionally replaced by the corresponding segments of the N protein of BCoV, a closely related group 2a coronavirus (43).

In that analysis, wild-type-like MHV recombinants bearing allowable BCoV N substitutions were selected via targeted RNA recombination between various donor RNAs and a temperature-sensitive MHV N mutant (30). The resulting collection of chimeric MHV-BCoV N proteins, a subset of which are shown in Fig. 1A, revealed that most portions of the N protein were interchangeable between the two species, with the possible exceptions of the amino terminus, the SR region, and the carboxy-terminal domain N3. However, the donor RNA that had been constructed to introduce BCoV N domain N3 into the MHV genome also contained a juxtaposition of BCoV and MHV elements in its 3′ UTR that we subsequently found to be lethal (25).

We now, therefore, reexamined the exchangeability of domain N3, this time using donor RNAs that left the MHV 3′ UTR intact and exactly replaced the coding region for domain N3 of the MHV N protein, as well as the upstream adjacent spacer B, with the homologous sequences from the BCoV N gene. Parallel constructs that contained spacer B and domain N3 from either another group 2a coronavirus, human coronavirus HKU1 (HCoV-HKU1) (64), or else the much more divergent group 2b coronavirus, SARS-CoV (56), were also made. To isolate the corresponding MHV mutants (and all other mutants discussed in the present work), we carried out recombination between donor RNAs and the feline-murine interspecies coronavirus fMHV (31). This reverse-genetic approach takes advantage of the powerful selection afforded by the reacquisition, by MHV recombinants, of the ability to grow in murine cells (20, 37). Recombinants containing substitutions of spacer B and domain N3 either from BCoV (mutant N-BN3) or from HCoV-HKU1 (mutant N-HKN3) were readily obtained, and we found them to be essentially phenotypically indistinguishable from the wild type (Fig. 1B). However, in multiple attempts, we were unable to isolate a mutant containing spacer B and domain N3 of the SARS-CoV N protein.

The N3 domain participates in homotypic interactions between N protein monomers (26). Additionally, N3 is responsible for the interaction of the N protein with the carboxy-terminal tail of the membrane protein (M) (27, 32, 62). In the latter context, it is noteworthy that neither the N-BN3 nor the N-HKN3 substitution mutant harbored any extra mutations in the cytoplasmic tail of the (MHV) M protein. The sequences of the N3 domains of BCoV and HCoV-HKU1, although substantially different from that for MHV, retain two conserved acidic residues (Fig. 1C, arrows) that have been shown to be essential for the interaction between the MHV N and M proteins (27, 62). In contrast, the SARS-CoV domain N3 sequence has diverged too far to be aligned with those of the group 2a coronaviruses (Fig. 1C), and it apparently cannot be functionally substituted for MHV domain N3.

The distinction between allowed and apparently unallowed N protein substitutions summarized in Fig. 1A presented a paradox, because the known interacting partners of the N protein are the M protein, viral RNA, and the N protein itself. The above-mentioned results indicated that associations with the M protein are equivalent in the MHV and BCoV N proteins, a conclusion that is reinforced by a previous demonstration that the cytoplasmic tails of the MHV and BCoV M proteins are, like the N3 domains, functionally interchangeable (12). Similarly, the RNA-binding abilities of the MHV and BCoV N proteins have been shown to be indistinguishable. The N protein of each species recognizes the highly homologous gRNA packaging signal of the other species (11). Moreover, another putative specific RNA ligand for N protein, the transcription-regulating sequence (23, 39), is identical in the two species. Finally, monomers of BCoV N protein ought, by definition, to interact correctly with other monomers of BCoV N protein, irrespective of whether they are in an MHV background. All of these considerations suggested that there must exist an as-yet-unknown additional critical function of N protein and, possibly, an unidentified interacting partner of N.

Substitution of the entire BCoV N gene in MHV. To more thoroughly explore the incompatibility of closely related N genes, we constructed a chimeric virus in which the entire BCoV N gene was forced to replace its MHV counterpart in an exact ORF-for-ORF substitution (Fig. 2A). The resulting BCoV N mutant was only minimally viable, forming plaques that were tiny in comparison to wild-type MHV (Fig. 2B). This mutant appeared similarly defective at all temperatures tested (33, 37, and 39°C), but it was more stable at 33°C, suggesting that higher temperatures created a greater selective pressure favoring the growth of revertants. Figure 2B shows plaques of a passage 1 stock of the initial isolate, designated Alb613, that was propagated only at 33°C. Additional independent isolates of the BCoV N mutant had an identical phenotype, but all subsequent work was carried out with Alb613.

To test whether the BCoV N protein was exerting a dominant negative effect in MHV, we constructed the BCoV N gene substitution in a genomic background that also contained a copy of the MHV N gene at an upstream site (Fig. 2A). The resulting MHV-BCoV N duplication mutant formed plaques that were far larger than those of the BCoV N mutant and were nearly as large as those of the wild type and those of an MHV-MHV N duplication mutant described previously (Fig. 2B) (26, 27). Importantly, sequence analysis of three independent MHV-BCoV N duplication mutants showed that none had acquired mutations at either of the two genomic sites at which reverting mutations for the BCoV N substitution were subsequently found. Therefore, rescue of the BCoV N mutant was entirely due to the added copy of the MHV N gene. This finding demonstrated that the BCoV N protein, when placed in an MHV background, was deficient in some critical function for viral replication that could be provided by MHV N protein.

Revertants of the BCoV N substitution mutant. Through three separate searches, we isolated a total of 14 independent revertants of the BCoV N mutant that had gained the ability to form plaques nearly as large as those of the wild type (Fig. 3A). Analysis of the entire (BCoV) N genes of these viruses revealed that 13 of them contained sequence changes, almost all of which mapped to the SR region of the N protein (Fig. 3B). The most common reverting mutation was S202L, which arose six separate times (in rev1, rev4, and rev10 through rev13). Other single point mutations were found at the same position (S202T in rev9) or at nearby residues (S205P in rev6 or S206I in rev2 and rev8). One revertant, rev7, had a pair of mutations, N197K and Q235L. Finally, a deletion of 3 residues was found in rev5 and a deletion of 12 residues in rev3. Two revertants had an additional coding mutation outside the SR region: T50I in rev12 and K435E in rev8. However, we judged these additional mutations to be extraneous because, in each case, there

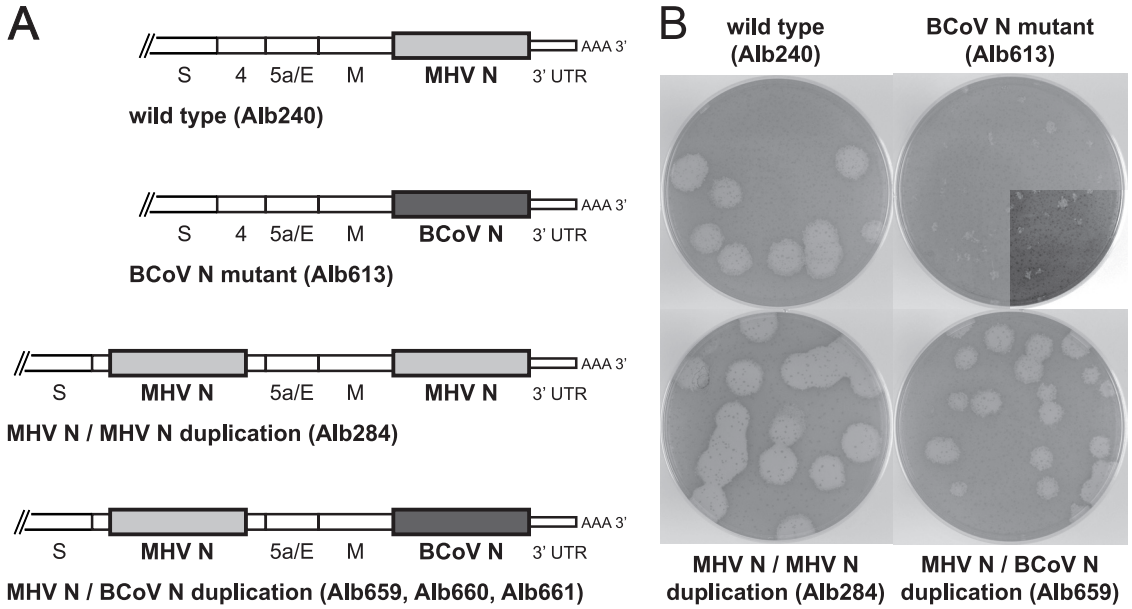

FIG. 2. Substitution of the entire BCoV N gene in place of the MHV N gene. (A) Schematic of the downstream ends of the genomes of wild-type MHV, the BCoV N substitution mutant, and derivatives of each in which the MHV N gene has been duplicated at an upstream position. (B) Plaques of the substitution and duplication mutants, compared to those of the wild type. Plaque titrations were carried out on L2 cells at 33°C. Monolayers were stained with neutral red at 120 h postinfection and photographed after 18 h of further incubation at 37°C. The lower right quadrant of the Alb613 photograph is shown with altered contrast to better allow visualization of the plaques of this mutant.

were other revertants for which a single mutation at the same position in the SR region was sufficient for reversion. The tight clustering of the reverting mutations suggested that the SR region is the major, and perhaps sole, component of the incompatibility of the BCoV N gene with MHV; this outcome was consistent with our previous domain exchange observations (Fig. 1A) (43). Importantly, the reverting mutations were localized to a region of N that was not clearly implicated in the known interactions of N protein with either M protein, RNA, or other molecules of N protein.

To ascertain the significance of the SR region mutations, two of them were reconstructed in the BCoV N gene. BCoV N substitution mutants containing either the S202L or the S205P mutation, all of which had large-plaque phenotypes, were recovered by targeted-RNA-recombination experiments at frequencies comparable to those of wild-type controls. Four independent recombinants of each type, examples of which are shown in Fig. 3C, were analyzed and were found to have the constructed mutation with no other changes in the BCoV N gene. These results confirmed that the S202L and S205P mutations were each able to compensate for the defect in the BCoV N mutant.

One of the revertants, rev14 (Fig. 3A), retained a completely wild-type BCoV N gene, indicating that it harbored a compensating mutation(s) outside the N gene. Contrary to our initial expectations, the other structural protein genes of this revertant were identical to those of wild-type MHV-A59. (A point mutation in the HE pseudogene was deemed irrelevant.) Sequencing of the entire genome of rev14 revealed that its only other difference from the wild-type sequence was a pair of closely spaced point mutations in the replicase gene, producing the changes T18I and A38V in the amino-terminal region of nsp3 (Fig. 4). Surprisingly, when we sequenced the first one-third of the nsp3 coding regions of all of the other 13 revertants, we found that six of them also had mutations in nsp3, in addition to their above-described N protein mutations. Most of these additional nsp3 changes were point mutations (in rev2, rev5, rev7, rev9, and rev11); however, for rev3, a 21-amino-acid deletion in nsp3 mirrored the 12-amino-acid deletion in the SR region of the N protein. For the revertants other than rev14, we have not yet established the significance of the observed nsp3 mutations, separate from the mutations in the BCoV N gene. It is noteworthy that all eight independent reconstructed S202L and S205P revertants (Fig. 3C) had no additional mutations in the first one-third of their nsp3 coding regions; thus, particular reverting mutations in the SR region of N were sufficient for reversion. However, in some cases, there may be additive effects between N and nsp3 mutations. This is suggested by the marginally larger plaques of rev11, which has S202L in N plus E5K in nsp3, than of rev4, which has solely S202L in N (Fig. 3A). In other cases, such as the pair of deletions in rev3, the nsp3 and N mutations may need to act in concert. With the exception of a second point mutation in rev2, all of the nsp3 mutations found in revertants of the BCoV N mutant mapped either within the amino-terminal ubiquitin-like domain (Ubl1) of nsp3 (53) or else in the adjacent acidic region (Ac) (Fig. 4). In total, our revertant analysis provides strong evidence for a previously unsuspected interaction between the N protein and nsp3 that is crucial to coronavirus replication.

Substitution of N protein SR regions from HCoV-HKU1 or SARS-CoV. To further examine the role of the SR region, we sought to replace this domain of the MHV N protein with its counterparts from group 2 coronaviruses other than BCoV.

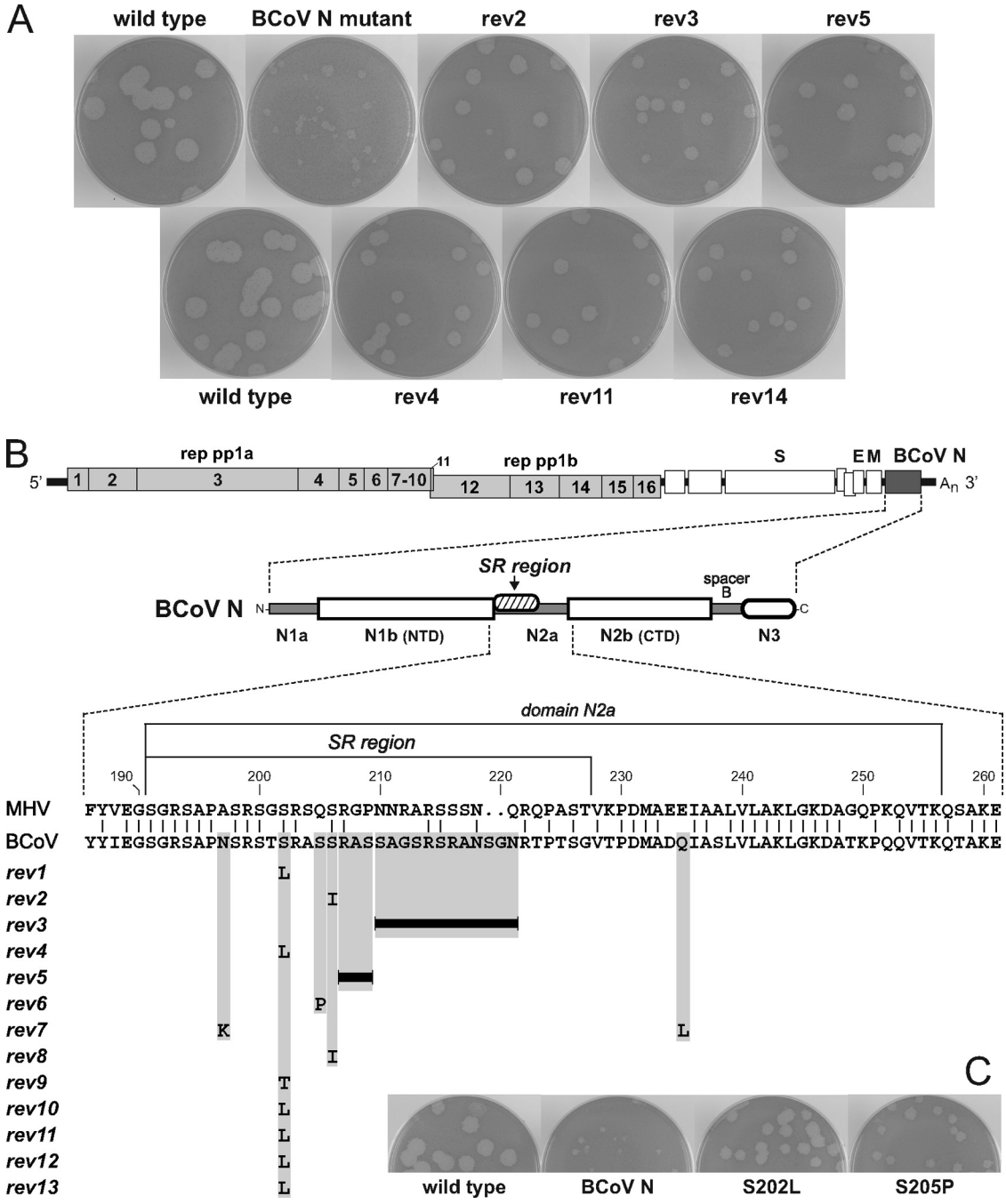

FIG. 3. Intragenic reverting mutations of the BCoV N substitution mutant. (A) Plaques of revertants of the BCoV N substitution mutant, compared to those of the original mutant and the wild type. Plaque titrations were carried out on L2 cells at 37°C. Monolayers were stained with neutral red at 72 h postinfection and photographed 18 h later; the upper and lower rows of photographs represent subsets of revertants obtained in two separate searches. (B) Reverting mutations mapped in the N gene. At the top is a schematic of the genome of the BCoV N substitution mutant; numbering in the replicase polyprotein gene (rep pp1a and rep pp1b) denotes the mature products nsp1-nsp16. Beneath the genome is an enlargement of the encoded BCoV N protein. The expanded segment shows an amino acid sequence alignment of the central regions of the N proteins of MHV and BCoV; the residue numbers are for the BCoV N sequence. Below the BCoV sequence are reverting mutations that were mapped in the N genes of 13 of the 14 independently isolated revertants; bars indicate deletions. (C) Plaques of reconstructed BCoV N revertants S202L and S205P, compared to those of the original mutant and the wild type. Plaque titrations were carried out on L2 cells at 33°C. Monolayers were stained with neutral red at 96 h postinfection and photographed 20 h later.

Initially, we constructed an MHV N mutant, designated HK-SR, containing a substitution of the SR region of HCoV-HKU1 (Fig. 5A). The HCoV-HKU1 N protein has an overall 67% amino acid sequence identity with the MHV N protein, a value comparable to the 70% identity between the BCoV and MHV N proteins. However, the homology between N protein SR regions is higher for HCoV-HKU1 and MHV than it is for BCoV and MHV (compare Fig. 5A and 3B). We isolated two

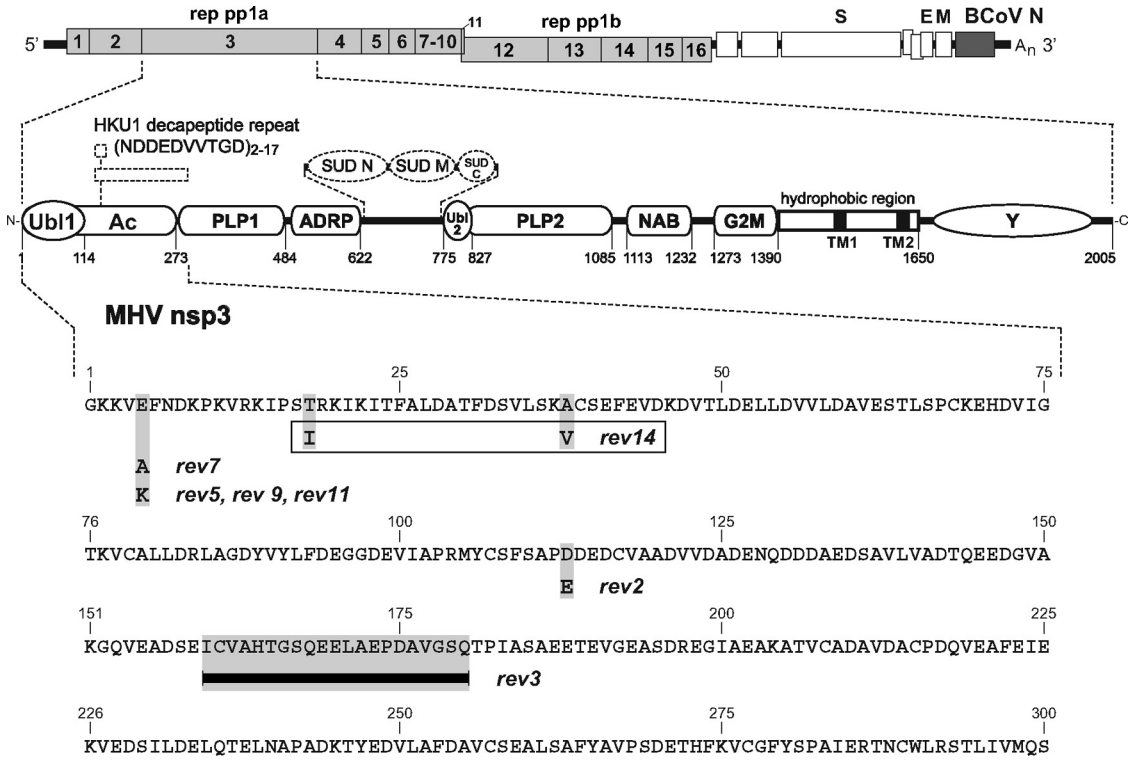

FIG. 4. Intergenic reverting mutations of the BCoV N substitution mutant. At the top is a schematic of the genome of the BCoV N substitution mutant; numbering in the replicase polyprotein gene (rep pp1a and rep pp1b) denotes the mature products nsp1 to nsp16. Beneath the genome is an enlargement of the encoded MHV nsp3. The residue numbers are those of the mature MHV nsp3 sequence; the first residue of nsp3 is residue 833 of the unprocessed replicase polyprotein. The schematic represents domains that have been identified for nsp3 of MHV or for homologous regions of nsp3 of other coronaviruses. The nomenclature for the domains of nsp3 is largely that of Neuman and coworkers (40): Ubl, ubiquitin-like domain; Ac, acidic region; PLP, papain-like proteinase; ADRP, ADP-ribose-1″-phosphatase; NAB, nucleic acid-binding domain; G2M, coronavirus group 2 marker domain; TM, transmembrane segment (41); Y, coronavirus highly conserved domain (75). Additionally, the dotted lines denote the positions and relative sizes of the N-terminal, middle, and C-terminal SARS-unique domains (SUD), which are found only in SARS-CoV nsp3 (56), and a variably repeated acidic decapeptide that occurs only in HCoV-HKU1 nsp3 (64, 65). The expanded segment shows the amino acid sequence of the amino terminus of MHV nsp3 with reverting mutations that were mapped in the nsp3 coding regions of 7 of the 14 independently isolated revertants. The bar indicates a deletion in rev3; rev2 also contains an additional point mutation, K563R, in the ADRP domain (not shown). The boxed mutations for rev14 are the only mutations occurring in the genome of that revertant; all other revertants shown also had mutations in the BCoV N protein (Fig. 3).

independent HK-SR recombinants, which were confirmed to contain exactly the expected sequence of the SR region substitution. Neither of these viruses displayed a significant phenotypic difference from wild-type MHV (data not shown). Additionally, each HK-SR recombinant retained an entirely wild-type sequence in the Ubl1-Ac region of nsp3, not only in the original isolate but also after six serial passages. Thus, the SR regions of HCoV-HKU1 and MHV operate equivalently, suggesting that the extended region of identity between the HCoV-HKU1 and MHV N proteins (corresponding to MHV N residues 201 through 215) is sufficient for the function furnished by the SR region.

For substitution of the SR region of the SARS-CoV N protein, a more complex pattern emerged. The overall amino acid sequence identity between the SARS-CoV and MHV N proteins is less than 35%, and the two proteins are highly divergent in the SR region (Fig. 5B). On the basis of the limited sequence identity of bounding segments, we designed a SARS-CoV SR region substitution construct, designated S-SR. However, in a total of five independent targeted-RNA-recombination trials, we were unable to isolate the corresponding viral mutant. Since these trials included controls in which wild-type donor RNAs yielded robust numbers of recombinants, our negative results can be taken to signify that the substitution in S-SR is lethal.

We were, nevertheless, able to obtain two independent recombinants, each of which harbored the S-SR substitution plus a secondary change in the SR region. One of these recombinants, Alb684, contained the adaptive mutation P217H; the other, Alb685, contained S215L (Fig. 5B). There were no additional mutations, in either Alb684 or Alb685, in the Ubl1-Ac region of nsp3. Both Alb684 and Alb685 formed plaques that were much smaller than those of the wild type although not as tiny as those of the BCoV N mutant, and both mutants grew markedly more slowly than did wild-type MHV. When we serially passaged Alb684 and Alb685, we noted increases in their growth rates by the sixth or seventh passage. Three large-plaque-forming revertants of each mutant were analyzed, and some were found to contain an additional mutation (S194F, S204Y, or T235N) in the SR region of the chimeric N protein (Fig. 5B). Remarkably, sequencing of the first one-third of the nsp3 coding region of the revertants revealed that all of them

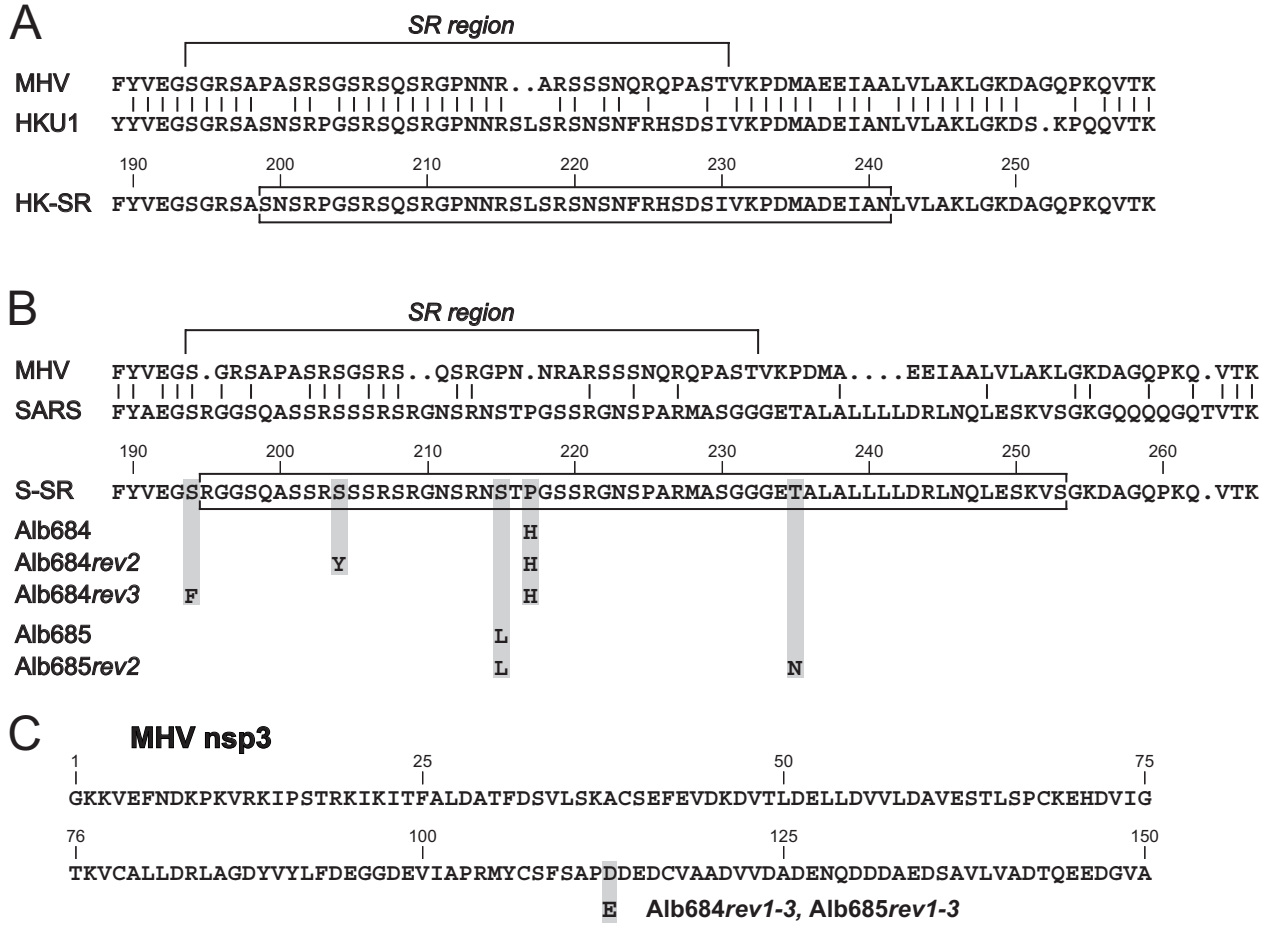

FIG. 5. Replacement of the SR region of the MHV N protein by the SR region of the HCoV-HKU1 or the SARS-CoV N protein. (A) Amino acid sequence alignment of the central regions of the N proteins of MHV and HCoV-HKU1. Beneath this is the corresponding region of the substitution mutant HK-SR, with the substituted segment boxed; the residue numbers are for the chimeric N protein sequence. (B) Amino acid sequence alignment of the central regions of the N proteins of MHV and SARS-CoV. Beneath this is the corresponding region of the designed substitution mutant S-SR, with the substituted segment boxed; the residue numbers are for the chimeric N protein sequence. Below the S-SR sequence are mutations that were found in the N genes of two independent S-SR recombinants, Alb684 and Alb685; Alb685 contains an additional mutation, G44V, in domain N1b (not shown). Also indicated are reverting mutations that were mapped in the N proteins of revertants of Alb684 and Alb685; Alb685rev3 contains an additional mutation, R406I, in spacer B (not shown). (C) Amino acid sequence of the amino terminus of MHV nsp3 showing a reverting mutation that was mapped in the nsp3 coding region of all of the isolated revertants of Alb684 and Alb685.

contained the mutation D113E at the Ubl1-Ac boundary in nsp3 (Fig. 5C). This same point mutation had previously been found in rev2 of the BCoV N mutant (Fig. 4). Thus, although the SARS-CoV SR region was not able to directly replace the corresponding segment of the MHV N protein, it could become functional through the acquisition of mutations in the SR region of N or in the amino-terminal region of nsp3. These results provided further genetic support for the existence of a critical association between the N protein and nsp3.

***In vitro* pulldown of N protein by the Ubl1-Ac fragment of nsp3.** To seek evidence complementary to our genetic results, we carried out GST pulldown assays. Toward this end, we bacterially expressed the Ubl1-Ac region of nsp3 (amino acids 1 to 273) (Fig. 4) as a carboxy-terminal GST fusion protein. GST-nsp3(1-273) was soluble and stable, and it exhibited a somewhat slower SDS-PAGE mobility than expected for its molecular mass (56 kDa), probably due to its high content of acidic residues (Fig. 6E and F). GST-nsp3(1-273), as well as control GST protein, was immobilized on glutathione affinity resin spin columns and then incubated with lysates from MHV-infected cells or from uninfected controls. Analysis of bound proteins showed that N protein was strongly retained by immobilized GST-nsp3(1-273), although we could also detect a weak background of nonspecific binding of N to GST or even to glutathione affinity resin alone (Fig. 6A and C). Since N protein is an RNA-binding protein, and since the Ubl1 domain of SARS-CoV nsp3 has been reported to have low-affinity RNA-binding activity (53), we performed the same set of pulldown assays using MHV-infected cell lysates that had been pretreated with RNase A. Under this condition, we found a marked increase of N protein binding to GST-nsp3(1-273) (Fig. 6B and D). Moreover, nonspecific binding of N to GST or to resin was reduced. These results demonstrated that a highly specific *in vitro* interaction exists between N protein and the Ubl1-Ac region of nsp3; this interaction is likely not to be mediated by a mutual affinity of the two proteins for RNA.

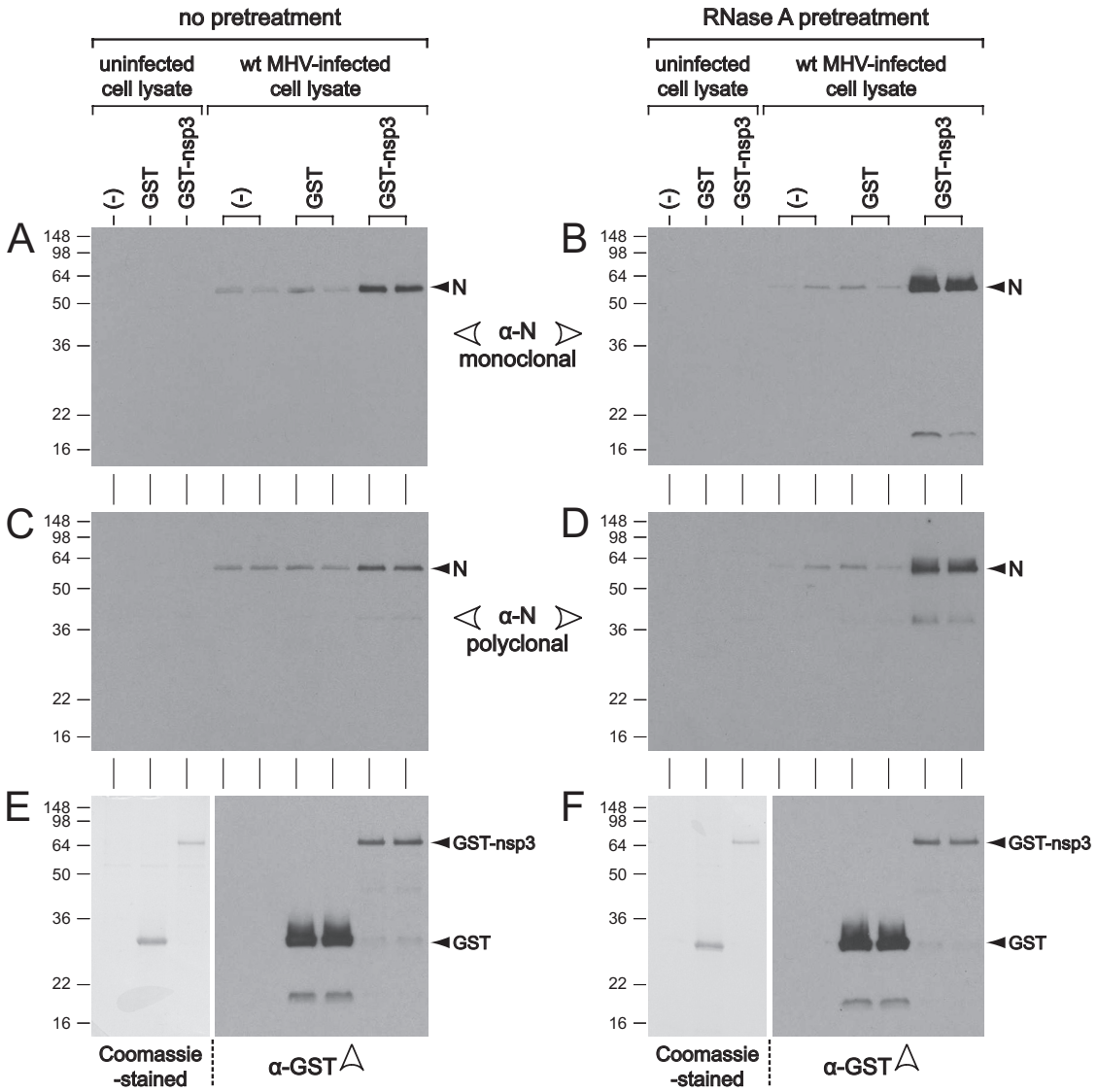

FIG. 6. Pulldown of N protein by the amino-terminal segment of nsp3. Expressed GST or GST-nsp3(1-273) fusion proteins were bound to glutathione affinity resin spin columns, as described in Materials and Methods; (−) denotes columns with resin alone. Columns were incubated with lysates from uninfected cells or from cells infected with wild-type MHV (Alb240) that either had been left untreated (A, C, E) or else had been pretreated by incubation with RNase A (B, D, F). Bound proteins were eluted with glutathione, and equal amounts of eluted material were analyzed using Western blots probed with anti-N (α-N) monoclonal antibody (A, B) directed against an epitope in domain N3 (27), anti-N polyclonal antibody (C, D), or anti-GST (α-GST) antibody (E, F). Eluted material was also analyzed by SDS-PAGE, followed by staining with Coomassie blue (E, F). Molecular mass standards (kDa) are indicated to the left of each panel.

Correlation of SR region function with the ability of N protein to enhance the infectivity of genomic RNA. One role for an obligatory association between N protein and nsp3 could be to localize gRNA to the replication compartment early in infection. Such a possibility suggested to us that the incompatibility that we discovered between the BCoV N protein and the MHV replicase is related to the previously observed requirement of N protein for optimal coronavirus replication (1, 6, 10, 51, 60, 69–71, 76). To test this hypothesis, we quantitated, by a direct plaque assay, the abilities of various synthetic N mRNAs to enhance infection initiated by MHV gRNA. We found that gRNA isolated from purified MHV virions was only minimally infectious when transfected into mouse L2 cells (Fig. 7A), consistent with our prior observations (36). In contrast, the inclusion of cotransfected MHV N mRNA caused a >40-fold increase in PFU obtained from the same amount of MHV gRNA. However, this enhancement was not brought about by cotransfection of MHV N mRNA containing knockout mutations early in the N ORF. The knockout mutations abolished translation of the N protein (Fig. 7B), while leaving intact the internal (I) gene, which is embedded within the N gene (17, 52). This result demonstrated that stimulation of gRNA infectivity is dependent upon translation of N protein (but not I protein) and that stimulation is not merely due to the provision, by added mRNA, of nonspecific protection against cellular RNase activity. A similar requirement for N protein,

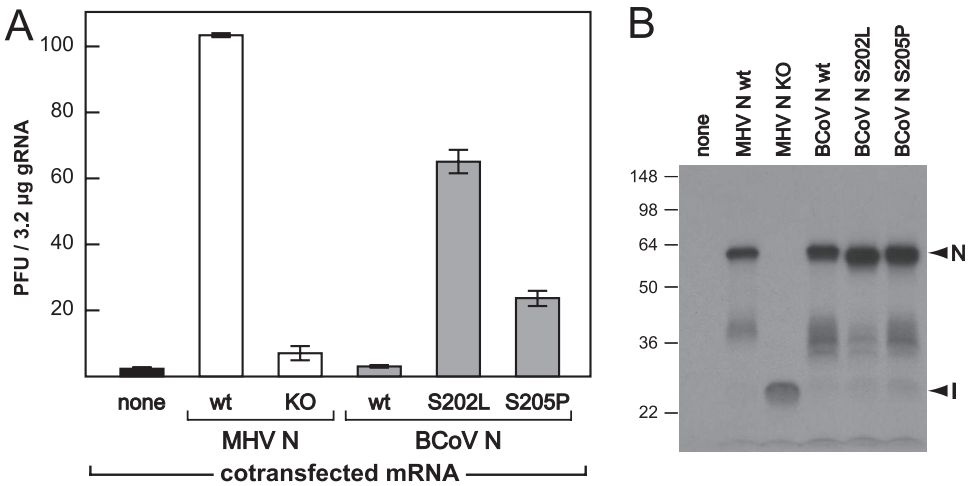

FIG. 7. Enhancement of the infectivity of MHV gRNA by cotransfected N mRNA. (A) L2 cells in suspension were transfected with MHV gRNA plus the indicated added synthetic N mRNA or plus a water control. The cotransfected N mRNAs included the MHV wild type (wt), the MHV knockout (KO), the BCoV wild type (wt), and BCoV point mutants (S202L and S205P). Transfected cells were seeded into dishes and overlaid with agar following attachment of cells; plaques were counted after 72 h of incubation at 37°C. Each histogram represents the mean infectious titer (± standard deviation) from three separate transfections. (B) *In vitro*-transcribed mRNAs were translated in a reticulocyte lysate system, and [^{35}S]methionine-labeled protein products were analyzed by SDS-PAGE, followed by fluorography. (Note that the MHV and BCoV N proteins contain 4 and 8 methionine residues, respectively.)

rather than RNA, has been shown for other coronavirus systems (1, 51).

In marked distinction to the efficacy of wild-type MHV mRNA, cotransfected wild-type BCoV mRNA was entirely unable to boost the infectivity of MHV gRNA (Fig. 7A). This outcome strongly suggests that MHV N protein is required for some early function in infection that cannot be provided by BCoV N protein, given that, later in infection, transfected gRNA eventually produces its own subgenomic mRNA encoding MHV N protein. To confirm the validity of this negative result, we extensively resequenced the plasmid from which synthetic BCoV mRNA was transcribed; additionally, we ascertained that BCoV mRNA was fully functional as a template for translation (Fig. 7B). Remarkably, high levels of enhancement of the infectivity of MHV gRNA could be restored through cotransfection of BCoV N mRNAs containing either of two single point mutations, S202L and S205P (Fig. 7A). These identical mutations were among the reverting mutations that we earlier found to be sufficient, without additional mutations in nsp3, to rescue the BCoV N mutant phenotype (Fig. 3 and 4). Taken together, our results demonstrate that a direct relationship exists between the N-nsp3 interaction and the requirement for N protein for optimal gRNA replication.

DISCUSSION

In the current study, we have provided extensive genetic evidence for a previously unsuspected interaction between the SR region of the MHV N protein and a component of the viral replicase complex, nsp3. The interaction was discovered as a consequence of the incompatibility of the BCoV N protein and the MHV replicase. Placement of the BCoV N gene into the MHV genome created a severely debilitated viral mutant that could be rescued by a reverting mutation either in the SR region of the N protein or in the Ubl1-Ac region of nsp3 or by mutations in both. We additionally demonstrated that insertion of the SR region of the SARS-CoV N protein into MHV similarly resulted in a defect that could be compensated for by the same two classes of reverting mutations. Moreover, we have corroborated our genetic results by biochemical evidence showing that an expressed nsp3 Ubl1-Ac construct binds selectively to N protein from infected cells and that this *in vitro* interaction is apparently not mediated by RNA. Finally, we have established that a correlation exists between the N-nsp3 interaction and a long-known, but unexplained, requirement for N protein to promote optimal infectivity of coronavirus gRNA.

It has been observed in a number of studies that a fraction of N protein colocalizes with replicase components early in coronavirus infections (14, 55, 58, 61). However, the identity of an nsp-interacting partner of N was not previously known. nsp3 is by far the largest of the replicase polyprotein products; in MHV, it constitutes some 2,005 amino acids. It comprises a perplexing concatenation of separate modules, which are arranged as globular domains joined by flexibly disordered linker segments (40) (Fig. 4). Structures have been solved for most of the globular domains of SARS-CoV nsp3 (8, 15, 47, 48, 53, 54, 59) and, in some cases, for homologs from other coronaviruses (45, 67). At the amino terminus of nsp3 is the above-mentioned ubiquitin-like domain, Ubl1, which is adjacent to the unstructured acidic region, Ac (53, 75). Downstream of Ac, in MHV nsp3, is PLP1, the first of two papain-like proteinases (PLPs) (3, 5), followed by a macrodomain (ADRP, previously called the X domain [75]), which has poly-ADP-ribose binding activity and ADP-ribose-1″-phosphatase activity (15, 45, 46, 48, 67). Next is a region whose sizes and sequences are highly variable among different coronaviruses; this region, in SARS-CoV nsp3, constitutes a "SARS-unique domain" (SUD) (56). Part of the SUD (SUD-M) embodies a second macrodomain (8, 59). The hypervariable region is followed by a second pa-

pain-like proteinase (PLP2) (4, 34), which contains a second ubiquitin-like fold (Ubl2) at its amino terminus. Further downstream is a low-affinity, nonspecific nucleic acid-binding domain (NAB) (54) and a domain that is present only in the group 2 coronaviruses (G2M) (40). Finally, at the carboxy terminus is sited the relatively well-conserved Y domain, which contains three potential metal-binding cysteine and histidine clusters (40, 75). Near the carboxy terminus, between G2M and Y, is a hydrophobic region containing either two or four transmembrane segments (28, 41); the resultant topology of nsp3, accordingly, places all of the above-described domains on the same (cytoplasmic) face of the membrane. nsp3 independently localizes to the endoplasmic reticulum during synthesis (24, 28, 41), and it accumulates at the highest density in convoluted membranes and double-membrane vesicles that form during coronavirus infection as the sites of active RNA replication and transcription (29). nsp3 has also been found as a minor constituent of purified virions of SARS-CoV (40).

Although speculative RNA synthesis functions for some of the nsp3 domains have been put forward, current evidence indicates that most of these domains serve accessory roles that may be important in pathogenesis (16, 18) but are likely to be dispensable for the core activities of the viral replicase. A number of considerations strongly suggest that the nsp3 coding region provided an adventitious genomic site for recombination of host material, which then evolved into luxury functions through gene duplication and divergence (8, 21, 40, 56, 59). First, despite its huge target size, no classical temperature-sensitive lethal mutations have yet been mapped to nsp3, although multiple examples of such mutations have been found in the far smaller coding regions of nsp4, -5, -10, -12, -14, -15, and -16 (9, 19, 50, 57). This sparsity of genetic lesions could imply that the essential portions of nsp3 are actually quite limited. Second, many of the modules of nsp3 are very poorly conserved, and some of them (NAB, G2M, and SUD) are unique to particular groups or subgroups of the coronavirus family or tolerate extensive deletion (72). Third, ablation of the ADRP phosphatase activity of the macrodomain, while attenuating in the host, does not affect viral replication in tissue culture (16, 46); additionally, not all coronavirus ADRP domains are able to bind poly-ADP-ribose (45). Finally, the specialized responsibility of the PLPs, the processing of merely the nsp1-2, nsp2-3, and nsp3-4 cleavage sites, has the appearance of an evolutionary afterthought, in contrast to the other 12 strictly conserved cleavages that are carried out by the main proteinase (nsp5). Moreover, the precise specificities and site overlaps of the PLPs have evolved independently in different coronavirus subgroups, and some coronaviruses (SARS-CoV and infectious bronchitis virus) thrive with only a single PLP (56, 74). Strikingly, it has been shown for MHV that a severely impaired PLP1 active site mutant can be rescued if the nsp1-2 and nsp2-3 cleavage sites are also eliminated (22).

In contrast to the apparently dispensable nature of much of nsp3, our results point to the amino-terminal segment, encompassing Ubl1 and Ac, as one region of the molecule that is critical, if not essential, for viral replication. This region is the locus for multiple independent intergenic reverting mutations of the BCoV N mutant (Fig. 4). The dramatically defective phenotype of the BCoV N mutant leads us to conclude that some fundamental process in MHV infection is dependent upon the association of N protein with nsp3. The genetic evidence for this N-nsp3 association is bolstered by our demonstration that expressed Ubl1-Ac protein specifically binds to N protein in GST pulldown assays (Fig. 6). Such an interaction was not previously detected by the use of yeast or mammalian two-hybrid techniques in broad-scale analyses of SARS-CoV-encoded proteins (42, 63). Interestingly, SARS-CoV nsp3 was very recently identified among a collection of viral and cellular proteins that were selected by the SARS-CoV envelope (E) protein in a tandem affinity purification procedure, and the E-nsp3 association was more finely mapped to the Ubl1-Ac region of nsp3 (2). The functional importance of the latter interaction is presently unclear.

Although much remains to be done to biochemically characterize the binding of N protein to nsp3, all of our genetic evidence maps this interaction to the SR region of the N molecule. The SR region of N is highly basic (Fig. 3B), in marked contrast to the overwhelmingly acidic Ubl1-Ac segment of nsp3 (Fig. 4). It is therefore possible that the nature of the N-nsp3 interaction is largely electrostatic. The net basic character of the SR region is, however, likely to be modified by phosphorylation. The coronavirus N protein is a serine/threonine phosphoprotein, and MHV and SARS-CoV N proteins expressed in mammalian cells have recently been shown to harbor multiple phosphorylated residues in their SR regions (44, 66); phosphorylation is a characteristic feature of the much larger domains of cellular SR proteins (73). It is noteworthy, also, that both the N protein SR region and the nsp3 Ac region are flexibly disordered linkers (7, 53). Thus, their mutual binding may bring about a more structured conformation that influences protein and RNA interactions of the neighboring domains of each molecule.

A potential mechanistic role for the N-nsp3 interaction emerges from our comparison of the levels of competence of various N protein mRNAs to stimulate the initiation of infection by transfected gRNA (Fig. 7). We found a direct correlation between the impaired functionality of BCoV N protein in an MHV background and that protein's failure to stimulate the infectivity of MHV gRNA. Conversely, revertants of BCoV N protein, which gained the capacity to function in MHV, also gained the ability to stimulate the infectivity of MHV gRNA. The basis of the necessity for N protein in coronavirus RNA synthesis in replicon systems has been investigated, but there is not yet agreement about whether N protein exerts a greater effect on RNA replication (51, 60) or on transcription (1, 76). One result from prior work that is consistent with our current findings is the observation that reporter gene expression from a replicon of HCoV-229E (a group 1 coronavirus) could be partially supported by cotransfected N mRNA from another group 1 coronavirus, porcine epidemic diarrhea virus. However, N mRNA from the more phylogenetically distant virus MHV, a group 2 coronavirus, was inert in that system (51).

During the normal course of infection, N protein is part of a helical nucleocapsid that is delivered from the virion to the cytoplasm, following receptor binding and membrane fusion events. For infections initiated by the transfection of naked gRNA, N is generally provided as cotransfected mRNA. Although the stimulatory effect of N mRNA is of practical importance for launching coronavirus reverse genetics systems that are based on full-length cDNAs (6, 10, 69–71), little work

has yet been done to dissect what is required of N protein for its role at the outset of infection. Very recently, it was shown, through the use of a cotransfection assay comparable to ours, that MHV N mRNA containing the domain N1b (NTD) mutation Y127A completely fails to support wild-type MHV gRNA infectivity (23). Since the Y127A mutation was demonstrated to severely impair RNA binding and was lethal in the whole virus, that result established that RNA-binding ability is important for the role of N protein in the initiation of infection. Our work indicates that, in order to be able to enhance the infectivity of gRNA, N protein must also be able to interact with nsp3. We propose that N is responsible for tethering gRNA to the newly translated replicase, via nsp3, as a prerequisite for the formation of an initiation complex at the 3′ end of the genome. Because the start of negative-strand RNA synthesis is the first step of both genome replication and transcription (49, 77), we would expect the N-nsp3 interaction to exert a major influence on both of these RNA-synthetic processes. This early function of N would not rule out additional roles that have been proposed for N protein to sustain ongoing transcription (22, 76) or translation (39) throughout the course of infection. However, the results reported here begin to elucidate a mechanism for initiation of infection that sets coronaviruses apart from almost all other positive-strand RNA viruses.

ACKNOWLEDGMENTS

We are grateful to Lili Kuo for help in isolating the BCoV N mutant. We thank John Fleming (University of Wisconsin, Madison, WI) for generously providing N monoclonal antibody J.3.3. We thank the Applied Genomics Technology Core Facility of the Wadsworth Center for DNA sequencing.

This work was supported by Public Health Service grant AI 64603 from the National Institutes of Health.

REFERENCES

1. **Almazan, F., C. Galan, and L. Enjuanes.** 2004. The nucleoprotein is required for efficient coronavirus genome replication. J. Virol. **78:**12683–12688.
2. **Alvarez, E., M. L. DeDiego, J. L. Nieto-Torres, J. M. Jiménez-Guardeño, L. Marcos-Villar, and L. Enjuanes.** 2010. The envelope protein of severe acute respiratory syndrome coronavirus interacts with the non-structural protein 3 and is ubiquitinated. Virology **402:**281–291.
3. **Baker, S. C., K. Yokomori, S. Dong, R. Carlisle, A. E. Gorbalenya, E. V. Koonin, and M. M. C. Lai.** 1993. Identification of the catalytic sites of a papain-like cysteine proteinase of murine coronavirus. J. Virol. **67:**6056–6063.
4. **Barretto, N., D. Jukneliene, K. Ratia, Z. Chen, A. D. Mesecar, and S. C. Baker.** 2005. The papain-like protease of severe acute respiratory syndrome coronavirus has deubiquitinating activity. J. Virol. **79:**15189–15198.
5. **Bonilla, P. J., S. A. Hughes, and S. R. Weiss.** 1997. Characterization of a second cleavage site and demonstration of activity in *trans* by the papain-like proteinase of the murine coronavirus mouse hepatitis virus strain A59. J. Virol. **71:**900–909.
6. **Casais, R., V. Thiel, S. G. Siddell, D. Cavanagh, and P. Britton.** 2001. Reverse genetics system for the avian coronavirus infectious bronchitis virus. J. Virol. **75:**12359–12369.
7. **Chang, C.-K., Y.-L. Hsu, Y.-H. Chang, F.-A. Chao, M.-C. Wu, Y.-S. Huang, C.-K. Hu, and T.-H. Huang.** 2009. Multiple nucleic acid binding sites and intrinsic disorder of severe acute respiratory syndrome coronavirus nucleocapsid protein: implications for ribonucleocapsid protein packaging. J. Virol. **83:**2255–2264.
8. **Chatterjee, A., M. A. Johnson, P. Serrano, B. Pedrini, J. S. Joseph, B. W. Neuman, K. Saikatendu, M. J. Buchmeier, P. Kuhn, and K. Wüthrich.** 2009. Nuclear magnetic resonance structure shows that the severe acute respiratory syndrome coronavirus-unique domain contains a macrodomain fold. J. Virol. **83:**1823–1836.
9. **Clementz, M. A., A. Kanjanahaluethai, T. E. O'Brien, and S. C. Baker.** 2008. Mutation in murine coronavirus replication protein nsp4 alters assembly of double membrane vesicles. Virology **375:**118–129.
10. **Coley, S. E., E. Lavi, S. G. Sawicki, L. Fu, B. Schelle, N. Karl, S. G. Siddell, and V. Thiel.** 2005. Recombinant mouse hepatitis virus strain A59 from cloned, full-length cDNA replicates to high titers in vitro and is fully pathogenic in vivo. J. Virol. **79:**3097–3106.
11. **Cologna, R., and B. G. Hogue.** 2000. Identification of a bovine coronavirus packaging signal. J. Virol. **74:**580–583.
12. **de Haan, C. A. M., L. Kuo, P. S. Masters, H. Vennema, and P. J. M. Rottier.** 1998. Coronavirus particle assembly: primary structure requirements of the membrane protein. J. Virol. **72:**6838–6850.
13. **de Haan, C. A. M., H. Volders, C. A. Koetzner, P. S. Masters, and P. J. M. Rottier.** 2002. Coronaviruses maintain viability despite dramatic rearrangements of the strictly conserved genome organization. J. Virol. **76:**12491–12493.
14. **Denison, M. R., W. J. M. Spaan, Y. van der Meer, C. A. Gibson, A. C. Sims, E. Prentice, and X. T. Lu.** 1999. The putative helicase of the coronavirus mouse hepatitis virus is processed from the replicase gene polyprotein and localizes in complexes that are active in viral RNA synthesis. J. Virol. **73:**6862–6871.
15. **Egloff, M. P., H. Malet, A. Putics, M. Heinonen, H. Dutartre, A. Frangeul, A. Gruez, V. Campanacci, C. Cambillau, J. Ziebuhr, T. Ahola, and B. Canard.** 2006. Structural and functional basis for ADP-ribose and poly(ADP-ribose) binding by viral macro domains. J. Virol. **80:**8493–8502.
16. **Eriksson, K. K., L. Cervantes-Barragán, B. Ludewig, and V. Thiel.** 2008. Mouse hepatitis virus liver pathology is dependent on ADP-ribose-1′′-phosphatase, a viral function conserved in the alpha-like supergroup. J. Virol. **82:**12325–12334.
17. **Fischer, F., D. Peng, S. T. Hingley, S. R. Weiss, and P. S. Masters.** 1997. The internal open reading frame within the nucleocapsid gene of mouse hepatitis virus encodes a structural protein that is not essential for viral replication. J. Virol. **71:**996–1003.
18. **Frieman, M., K. Ratia, R. E. Johnston, A. D. Mesecar, and R. S. Baric.** 2009. Severe acute respiratory syndrome coronavirus papain-like protease ubiquitin-like domain and catalytic domain regulate antagonism of IRF3 and NF-kappaB signaling. J. Virol. **83:**6689–6705.
19. **Fu, K., and R. S. Baric.** 1994. Map locations of mouse hepatitis virus temperature-sensitive mutants: confirmation of variable rates of recombination. J. Virol. **68:**7458–7466.
20. **Goebel, S. J., B. Hsue, T. F. Dombrowski, and P. S. Masters.** 2004. Characterization of the RNA components of a putative molecular switch in the 3′ untranslated region of the murine coronavirus genome. J. Virol. **78:**669–682.
21. **Gorbalenya, A. E., L. Enjuanes, J. Ziebuhr, and E. J. Snijder.** 2006. Nidovirales: evolving the largest RNA virus genome. Virus Res. **117:**17–37.
22. **Graham, R. L., and M. R. Denison.** 2006. Replication of murine hepatitis virus is regulated by papain-like proteinase 1 processing of nonstructural proteins 1, 2, and 3. J. Virol. **80:**11610–11620.
23. **Grossoehme, N. E., L. Li, S. C. Keane, P. Liu, C. E. Dann III, J. L. Leibowitz, and D. P. Giedroc.** 2009. Coronavirus N protein N-terminal domain (NTD) specifically binds the transcriptional regulatory sequence (TRS) and melts TRS-cTRS RNA duplexes. J. Mol. Biol. **394:**544–557.
24. **Harcourt, B. H., D. Jukneliene, A. Kanjanahaluethai, J. Bechill, K. M. Severson, C. M. Smith, P. A. Rota, and S. C. Baker.** 2004. Identification of severe acute respiratory syndrome coronavirus replicase products and characterization of papain-like protease activity. J. Virol. **78:**13600–13612.
25. **Hsue, B., and P. S. Masters.** 1997. A bulged stem-loop structure in the 3′ untranslated region of the genome of the coronavirus mouse hepatitis virus is essential for replication. J. Virol. **71:**7567–7578.
26. **Hurst, K. R., C. A. Koetzner, and P. S. Masters.** 2009. Identification of in vivo-interacting domains of the murine coronavirus nucleocapsid protein. J. Virol. **83:**7221–7234.
27. **Hurst, K. R., L. Kuo, C. A. Koetzner, R. Ye, B. Hsue, and P. S. Masters.** 2005. A major determinant for membrane protein interaction localizes to the carboxy-terminal domain of the mouse coronavirus nucleocapsid protein. J. Virol. **79:**13285–13297.
28. **Kanjanahaluethai, A., Z. Chen, D. Jukneliene, and S. C. Baker.** 2007. Membrane topology of murine coronavirus replicase nonstructural protein 3. Virology **361:**391–401.
29. **Knoops, K., M. Kikkert, S. H. Worm, J. C. Zevenhoven-Dobbe, Y. van der Meer, A. J. Koster, A. M. Mommaas, and E. J. Snijder.** 2008. SARS-coronavirus replication is supported by a reticulovesicular network of modified endoplasmic reticulum. PLoS Biol. **6:**e226.
30. **Koetzner, C. A., M. M. Parker, C. S. Ricard, L. S. Sturman, and P. S. Masters.** 1992. Repair and mutagenesis of the genome of a deletion mutant of the coronavirus mouse hepatitis virus by targeted RNA recombination. J. Virol. **66:**1841–1848.
31. **Kuo, L., G.-J. Godeke, M. J. B. Raamsman, P. S. Masters, and P. J. M. Rottier.** 2000. Retargeting of coronavirus by substitution of the spike glycoprotein ectodomain: crossing the host cell species barrier. J. Virol. **74:**1393–1406.
32. **Kuo, L., and P. S. Masters.** 2002. Genetic evidence for a structural interaction between the carboxy termini of the membrane and nucleocapsid proteins of mouse hepatitis virus. J. Virol. **76:**4987–4999.
33. **Kuo, L., and P. S. Masters.** 2003. The small envelope protein E is not essential for murine coronavirus replication. J. Virol. **77:**4597–4608.

34. **Lindner, H. A., N. Fotouhi-Ardakani, V. Lytvyn, P. Lachance, T. Sulea, and R. Ménard.** 2005. The papain-like protease from the severe acute respiratory syndrome coronavirus is a deubiquitinating enzyme. J. Virol. **79:**15199–15208.
35. **Masters, P. S.** 2006. The molecular biology of coronaviruses. Adv. Virus Res. **66:**193–292.
36. **Masters, P. S., C. A. Koetzner, C. A. Kerr, and Y. Heo.** 1994. Optimization of targeted RNA recombination and mapping of a novel nucleocapsid gene mutation in the coronavirus mouse hepatitis virus. J. Virol. **68:**328–337.
37. **Masters, P. S., and P. J. M. Rottier.** 2005. Coronavirus reverse genetics by targeted RNA recombination. Curr. Top. Microbiol. Immunol. **287:**133–159.
38. **Mizutani, S., and R. J. Colonno.** 1985. In vitro synthesis of an infectious RNA from cDNA clones of human rhinovirus type 14. J. Virol. **56:**628–632.
39. **Nelson, G. W., S. A. Stohlman, and S. M. Tahara.** 2000. High affinity interaction between nucleocapsid protein and leader/intergenic sequence of mouse hepatitis virus RNA. J. Gen. Virol. **81:**181–188.
40. **Neuman, B. W., J. S. Joseph, K. S. Saikatendu, P. Serrano, A. Chatterjee, M. A. Johnson, L. Liao, J. P. Klaus, J. R. Yates III, K. Wüthrich, R. C. Stevens, M. J. Buchmeier, and P. Kuhn.** 2008. Proteomics analysis unravels the functional repertoire of coronavirus nonstructural protein 3. J. Virol. **82:**5279–5294.
41. **Oostra, M., M. C. Hagemeijer, M. van Gent, C. P. Bekker, E. G. te Lintelo, P. J. M Rottier, and C. A. de Haan.** 2008. Topology and membrane anchoring of the coronavirus replication complex: not all hydrophobic domains of nsp3 and nsp6 are membrane spanning. J. Virol. **82:**12392–12405.
42. **Pan, J., X. Peng, Y. Gao, Z. Li, X. Lu, Y. Chen, M. Ishaq, D. Liu, M. L. DeDiego, L. Enjuanes, and D. Guo.** 2008. Genome-wide analysis of protein-protein interactions and involvement of viral proteins in SARS-CoV replication. PLoS One **3:**e3299.
43. **Peng, D., C. A. Koetzner, T. McMahon, Y. Zhu, and P. S. Masters.** 1995. Construction of murine coronavirus mutants containing interspecies chimeric nucleocapsid proteins. J. Virol. **69:**5475–5484.
44. **Peng, T. Y., K. R. Lee, and W. Y. Tarn.** 2008. Phosphorylation of the arginine/serine dipeptide-rich motif of the severe acute respiratory syndrome coronavirus nucleocapsid protein modulates its multimerization, translation inhibitory activity and cellular localization. FEBS J. **275:**4152–4163.
45. **Piotrowski, Y., G. Hansen, A. L. Boomaars-van der Zanden, E. J. Snijder, A. E. Gorbalenya, and R. Hilgenfeld.** 2009. Crystal structures of the X-domains of a Group-1 and a Group-3 coronavirus reveal that ADP-ribose-binding may not be a conserved property. Protein Sci. **18:**6–16.
46. **Putics, A., W. Filipowicz, J. Hall, A. E. Gorbalenya, and J. Ziebuhr.** 2005. ADP-ribose-1″-monophosphatase: a conserved coronavirus enzyme that is dispensable for viral replication in tissue culture. J. Virol. **79:**12721–12731.
47. **Ratia, K., K. S. Saikatendu, B. D. Santarsiero, N. Barretto, S. C. Baker, R. C. Stevens, and A. D. Mesecar.** 2006. Severe acute respiratory syndrome coronavirus papain-like protease: structure of a viral deubiquitinating enzyme. Proc. Natl. Acad. Sci. U. S. A. **103:**5717–5722.
48. **Saikatendu, K. S., J. S. Joseph, V. Subramanian, T. Clayton, M. Griffith, K. Moy, J. Velasquez, B. W. Neuman, M. J. Buchmeier, R. C. Stevens, and P. Kuhn.** 2005. Structural basis of severe acute respiratory syndrome coronavirus ADP-ribose-1″-phosphate dephosphorylation by a conserved domain of nsP3. Structure **13:**1665–1675.
49. **Sawicki, S. G., D. L. Sawicki, and S. G. Siddell.** 2007. A contemporary view of coronavirus transcription. J. Virol. **81:**20–29.
50. **Sawicki, S. G., D. L. Sawicki, D. Younker, Y. Meyer, V. Thiel, H. Stokes, and S. G. Siddell.** 2005. Functional and genetic analysis of coronavirus replicase-transcriptase proteins. PLoS Pathog. **1:**e39.
51. **Schelle, B., N. Karl, B. Ludewig, S. G. Siddell, and V. Thiel.** 2005. Selective replication of coronavirus genomes that express nucleocapsid protein. J. Virol. **79:**6620–6630.
52. **Senanayake, S. D., M. A. Hofmann, J. L. Maki, and D. A. Brian.** 1992. The nucleocapsid protein gene of bovine coronavirus is bicistronic. J. Virol. **66:**5277–5283.
53. **Serrano, P., M. A. Johnson, M. S. Almeida, R. Horst, T. Herrmann, J. S. Joseph, B. W. Neuman, V. Subramanian, K. S. Saikatendu, M. J. Buchmeier, R. C. Stevens, P. Kuhn, and K. Wüthrich.** 2007. Nuclear magnetic resonance structure of the N-terminal domain of nonstructural protein 3 from the severe acute respiratory syndrome coronavirus. J. Virol. **81:**12049–12060.
54. **Serrano, P., M. A. Johnson, A. Chatterjee, B. W. Neuman, J. S. Joseph, M. J. Buchmeier, P. Kuhn, and K. Wüthrich.** 2009. NMR structure of the nucleic acid-binding domain of the SARS coronavirus nonstructural protein 3. J. Virol. **83:**12998–13008.
55. **Sims, A. C., J. Ostermann, and M. R. Denison.** 2000. Mouse hepatitis virus replicase proteins associate with two distinct populations of intracellular membranes. J. Virol. **74:**5647–5654.
56. **Snijder, E. J., P. J. Bredenbeek, J. C. Dobbe, V. Thiel, J. Ziebuhr, L. L. M. Poon, Y. Guan, M. Rozanov, W. J. M. Spaan, and A. E. Gorbalenya.** 2003. Unique and conserved features of genome and proteome of SARS coronavirus, an early split-off from the coronavirus group 2 lineage. J. Mol. Biol. **331:**991–1004.
57. **Sparks, J. S., E. F. Donaldson, X. Lu, R. S. Baric, and M. R. Denison.** 2008. A novel mutation in murine hepatitis virus nsp5, the viral 3C-like proteinase, causes temperature-sensitive defects in viral growth and protein processing. J. Virol. **82:**5999–6008.
58. **Stertz, S., M. Reichelt, M. Spiegel, T. Kuri, L. Martínez-Sobrido, A. García-Sastre, F. Weber, and G. Kochs.** 2007. The intracellular sites of early replication and budding of SARS-coronavirus. Virology **361:**304–315.
59. **Tan, J., C. Vonrhein, O. S. Smart, G. Bricogne, M. Bollati, Y. Kusov, G. Hansen, J. R. Mesters, C. L. Schmidt, and R. Hilgenfeld.** 2009. The SARS-unique domain (SUD) of SARS coronavirus contains two macrodomains that bind G-quadruplexes. PLoS Pathog. **5:**e1000428.
60. **Thiel, V., J. Herold, B. Schelle, and S. G. Siddell.** 2001. Viral replicase gene products suffice for coronavirus discontinuous transcription. J. Virol. **75:**6676–6681.
61. **van der Meer, Y., E. J. Snijder, J. C. Dobbe, S. Schleich, M. R. Denison, W. J. M. Spaan, and J. K. Locker.** 1999. Localization of mouse hepatitis virus nonstructural proteins and RNA synthesis indicates a role for late endosomes in viral replication. J. Virol. **73:**7641–7657.
62. **Verma, S., V. Bednar, A. Blount, and B. G. Hogue.** 2006. Identification of functionally important negatively charged residues in the carboxy end of mouse hepatitis coronavirus A59 nucleocapsid protein. J. Virol. **80:**4344–4355.
63. **von Brunn, A., C. Teepe, J. C. Simpson, R. Pepperkok, C. C. Friedel, R. Zimmer, R. Roberts, R. Baric, and J. Haas.** 2007. Analysis of intraviral protein-protein interactions of the SARS coronavirus ORFeome. PLoS One **2:**e459.
64. **Woo, P. C. Y., S. K. P. Lau, C.-M. Chu, K.-H. Chan, H.-W. Tsoi, Y. Huang, B. H. L. Wong, R. W. S. Poon, J. J. Cai, W.-K. Luk, L. L. M. Poon, S. S. Y. Wong, Y. Guan, J. S. M. Peiris, and K.-Y. Yuen.** 2005. Characterization and complete genome sequence of a novel coronavirus, coronavirus HKU1, from patients with pneumonia. J. Virol. **79:**884–895.
65. **Woo, P. C., S. K. Lau, C. C. Yip, Y. Huang, H. W. Tsoi, K. H. Chan, and K. Y. Yuen.** 2006. Comparative analysis of 22 coronavirus HKU1 genomes reveals a novel genotype and evidence of natural recombination in coronavirus HKU1. J. Virol. **80:**7136–7145.
66. **Wu, C. H., S. H. Yeh, Y. G. Tsay, Y. H. Shieh, C. L. Kao, Y. S. Chen, S. H. Wang, T. J. Kuo, D. S. Chen, and P. J. Chen.** 2009. Glycogen synthase kinase-3 regulates the phosphorylation of severe acute respiratory syndrome coronavirus nucleocapsid protein and viral replication. J. Biol. Chem. **284:**5229–5239.
67. **Xu, Y., L. Cong, C. Chen, L. Wei, Q. Zhao, X. Xu, Y. Ma, M. Bartlam, and Z. Rao.** 2009. Crystal structures of two coronavirus ADP-ribose-1″-monophosphatases and their complexes with ADP-ribose: a systematic structural analysis of the viral ADRP domain. J. Virol. **83:**1083–1092.
68. **Ye, R., C. Montalto-Morrison, and P. S. Masters.** 2004. Genetic analysis of determinants for spike glycoprotein assembly into murine coronavirus virions: distinct roles for charge-rich and cysteine-rich regions of the endodomain. J. Virol. **78:**9904–9917.
69. **Yount, B., K. M. Curtis, and R. S. Baric.** 2000. Strategy for systematic assembly of large RNA and DNA genomes: transmissible gastroenteritis virus model. J. Virol. **74:**10600–10611.
70. **Yount, B., K. M. Curtis, E. A. Fritz, L. E. Hensley, P. B. Jahrling, E. Prentice, M. R. Denison, T. W. Geisbert, and R. S. Baric.** 2003. Reverse genetics with a full-length infectious cDNA of severe acute respiratory syndrome coronavirus. Proc. Natl. Acad. Sci. U. S. A. **100:**12995–13000.
71. **Yount, B., M. R. Denison, S. R. Weiss, and R. S. Baric.** 2002. Systematic assembly of a full-length infectious cDNA of mouse hepatitis virus strain A59. J. Virol. **76:**11065–11078.
72. **Yuan, J., C.-C. Hon, Y. Li, D. Wang, G. Xu, H. Zhang, P. Zhou, L. L. M. Poon, T. T.-Y. Lam, F. C.-C. Leung, and Z. Shi.** 2010. Intraspecies diversity of SARS-like coronaviruses in Rhinolophus sinicus and its implications for the origin of SARS coronaviruses in humans. J. Gen. Virol. **91:**1058–1062.
73. **Zhong, X. Y., P. Wang, J. Han, M. G. Rosenfeld, and X. D. Fu.** 2009. SR proteins in vertical integration of gene expression from transcription to RNA processing to translation. Mol. Cell **35:**1–10.
74. **Ziebuhr, J.** 2005. The coronavirus replicase. Curr. Top. Microbiol. Immunol. **287:**57–94.
75. **Ziebuhr, J., V. Thiel, and A. E. Gorbalenya.** 2001. The autocatalytic release of a putative RNA virus transcription factor from its polyprotein precursor involves two paralogous papain-like proteases that cleave the same peptide bond. J. Biol. Chem. **276:**33220–33232.
76. **Zúñiga, S., J. L. Cruz, I. Sola, P. A. Mateos-Gómez, L. Palacio, and L. Enjuanes.** 2010. Coronavirus nucleocapsid protein facilitates template switching and is required for efficient transcription. J. Virol. **84:**2169–2175.
77. **Züst, R., T. B. Miller, S. J. Goebel, V. Thiel, and P. S. Masters.** 2008. Genetic interactions between an essential 3′ *cis*-acting RNA pseudoknot, replicase gene products, and the extreme 3′ end of the mouse coronavirus genome. J. Virol. **82:**1214–1228.